Materials Research Bulletin 61 (2014) 130–135

Contents lists available at ScienceDirect

Materials Research Bulletin

journal homepage: www.elsevier.com/locate/matresbu

Phase transitions of $BaTi_{0.9}Rh_{0.1}O_{3\pm\delta}$ perovskite-type oxides under reducing environments

G.C.Mondragón Rodríguez [a,*], Y. Gönüllü [b], Davide Ferri [c], Arnim Eyssler [d], Eugenio Otal [e], B. Saruhan [a]

[a] German Aerospace Center (DLR), Institute of Materials Research, Linder Hoehe, D-51147 Cologne, Germany
[b] Institute of Inorganic Chemistry, University of Cologne, Germany
[c] Paul Scherrer Institut, CH-5232 Villigen PSI, Switzerland
[d] Empa, Swiss Federal Laboratories for Materials Science and Technology, Lab. for Solid State Chemistry and Catalysis, Ueberlandstrasse 129, CH-8600 Dübendorf, Switzerland
[e] UTN-Facultad Regional Santa Cruz, Av. Inmigrantes 555, Río Gallegos, 9400 Santa Cruz, Argentina

ARTICLE INFO

Article history:
Received 9 January 2014
Received in revised form 22 September 2014
Accepted 1 October 2014
Available online 5 October 2014

Keywords:
Perovskite
Chemical synthesis
XAFS
Microstructure

ABSTRACT

Perovskite-type oxides of composition $BaTi_{0.9}Rh_{0.1}O_{3\pm\delta}$ were prepared following a new chemical route that avoids the formation of hydroxyl species and precipitation, and allows the homogeneous distribution of Rh in the final mixed metal oxide. The high dispersion of Rh and the formation of the solid solution between Rh and the $BaTiO_3$ perovskite is confirmed by means of X-ray diffraction (XRD) and extended X-ray absorption fine structure spectroscopy (EXAFS). The presence of Rh stabilized the hexagonal $BaTi_{0.9}Rh_{0.1}O_{3\pm\delta}$ phase, which decomposes into barium orthotitanate ($BaTi_2O_4$) and metallic Rh° in reducing environment. This phase transition starts already at 700 °C and is only partially completed at 900 °C suggesting that part of the Rh present in the perovskite lattice might not be easily reduced by hydrogen. These aspects and further open questions are discussed.

© 2014 Elsevier Ltd. All rights reserved.

1. Introduction

The interest for doping perovskite-type oxides with precious metals such as Pt, Pd and Rh to improve their thermal resistance and catalytic properties started in the early 1970s [1]. Rhodium containing perovskite oxides such as $LaRhO_3$ and $La_{0.8}K_{0.2}Mn_{0.9}Rh_{0.1}O_3$ were tested for CO-oxidation and NO-reduction. A very high CO-oxidation potential and preferential selectivity to NH_3 during the reduction of NO were observed on these perovskite catalysts. An improvement of the catalytic activity of $La_{0.7}Pb_{0.3}Mn_{1-x}Ru_xO_3$ and $La_{0.8}K_{0.2}Mn_{1-x}Ru_xO_3$ upon reduction treatment was also reported. Ruthenium (Ru) particles were found upon prolonged reduction between 500 °C and 600 °C, but the good catalytic activity performance was attributed to the synergy between the perovskite and the metal. However, Voorhoeve [1] concluded that "these kinds of catalysts may face some practical problems due to the degree of mobility of the noble metal specially Ru, which may lead to agglomeration and evaporation", but excluded other metals such as Rh, Pt, and Pd.

Almost 30 years later, researchers at Daihatsu reported that only a small fraction of precious metals such as Pd, Rh, and Pt dissolved in different perovskite compositions can be reintegrated into their structure [2]. Precious metals such as Pd, Rh, and Pt atomically incorporated in perovskite oxide structures are reduced in CO and H_2 gases to form a metallic phase (Rh°, Pt°, Pd°). These metallic nanoparticles reversibly integrate into the perovskite lattice under oxidizing conditions. These phase transitions have been thoroughly studied and demonstrated for palladium in $LaFe_{0.95}Pd_{0.05}O_3$ and $LaFe_{0.57}Co_{0.38}PdO_3$ catalysts [3–6]. Similar perovskite compositions have been synthesized and tested for H_2-SCR (selective catalytic reduction) of NO_x [7,8] and methane oxidation [9,10]. Rh- and Pt-containing perovskite-type oxides have been less studied. Detailed studies are available for $LaFe_{0.95}Rh_{0.05}O_3$, $CaTi_{0.95}Rh_{0.05}O_3$, $LaFe_{0.95}Pt_{0.05}O_3$, and $CaTi_{0.95}Pt_{0.05}O_3$ [2,11,12]. The so called "self-regenerative" effect of Rh has also been reported for $LaAlO_3$, $CaZrO_3$, $SrTiO_3$, $BaZrO_3$, and $BaTiO_3$ [11]. Among these perovskite oxides, $BaTi_{0.95}Rh_{0.05}O_3$ displayed the best self-regenerative performance [11], but no further explanation was provided for the underlying mechanism. In a

* Corresponding author. Tel.: +49 02203 601 3869; fax: +49 02203 696480.
E-mail address: guillermo.mondragon-rodriguez@dlr.de (G.C.M. Rodríguez).

http://dx.doi.org/10.1016/j.materresbull.2014.10.007
0025-5408/© 2014 Elsevier Ltd. All rights reserved.

previous study, we found a new Rh-segregation mechanism involving the phase transition of the perovskite oxide into an orthorhombic phase upon reduction at 900 °C [13].

This study aims at obtaining a deeper insight into the mechanism of formation of the Rh-containing perovskite oxide and the segregation of Rh under reducing conditions. Rh-containing perovskite-type oxides, $BaTi_{0.9}Rh_{0.1}O_{3\pm\delta}$, were synthesized by a wet-chemistry method [13]. Samples were reduced at 700, 800 and 900 °C to promote the reduction and diffusion of Rh in order to understand the mechanism of phase transitions during Rh segregation. The reduced samples were carefully analyzed by FE-SEM, XRD, EXAFS and H_2-TPR. For reference purpose, Rh-free samples and Rh supported on $BaTiO_3$ (Rh–$BaTiO_3$) and TiO_2 (Rh–TiO_2) were treated and analyzed under similar reduction conditions.

2. Experimental

2.1. Synthesis

Barium acetate, titanium isopropoxide and rhodium nitrate are employed as metal precursors to prepare $BaTi_{0.9}Rh_{0.1}O_{3\pm\delta}$. Barium acetate (98% Chempur) is dissolved in acetic acid to achieve a concentration of 0.63 mol/l and Ti(IV) isopropoxide (99.999% Aldrich) is diluted with isopropanol and acetyl acetone (99% solution, Merck) Ti-isopropoxide:isopropanol:acetyl acetone = 1:3.75:2.5). The Ba and Ti solutions are mixed in stoichiometric concentrations followed by addition of the corresponding amount of $Rh(NO_3)_3$ (12.5 wt% Rh solution, Chempur) under constant stirring. A transparent solution is obtained with this synthesis method. The solvents are evaporated under constant stirring at room temperature, followed by calcination at 1000 °C for 5 h.

For comparison, two reference samples are prepared by impregnation of $BaTiO_3$ (designated as Rh–$BaTiO_3$) and TiO_2 (Rh–TiO_2) with $Rh(NO_3)_3$. For Rh–$BaTiO_3$, the Ba-acetate and Ti-isopropoxide sols are mixed together, dried and calcined in air at 1000 °C for 5 h. The resulting $BaTiO_3$ is mixed with the corresponding amount of Rh-nitrate aqueous solution to achieve 10 wt% Rh. Similarly, commercial TiO_2 (chemical grade, Merck) is homogeneously mixed with corresponding amount of the Rh $(NO_3)_3$ aqueous solution to obtain 10 wt% Rh loading. After solvent evaporation at room temperature both Rh–$BaTiO_3$ and Rh–TiO_2 precursors are calcined in air at 1000 °C for 5 h. The chemical composition of the samples is reported elsewhere [13].

The prepared $BaTi_{0.9}Rh_{0.1}O_{3\pm\delta}$ ($x = 0.1$) samples were reduced in 2.5 vol.% H_2 at atmospheric pressure at 700, 800 and 900 °C in order to study their redox properties. The temperature was raised to the annealing temperature at a heating rate of 10 °C × min^{-1} followed by a dwell time of 30 min. Cooling to room temperature was carried out over 3–4 h under the same reducing feed to maintain the reduced state.

2.2. Characterization methods

All samples were analyzed by the X-ray diffraction (XRD) and scanning electron microscopy (SEM). The XRD was employed to analyze the crystal structure and the phase composition of the samples. XRD diffraction patterns were obtained with a Siemens D5000 diffractometer using CuKα radiation ($\lambda = 1.54178$). The XRD patterns were assigned upon comparison with the JCPDS database using the EVA program (Bruker AXS). The XRD data of the perovskites for Rietveld refinement calculations were collected from $2\theta = 20°$ to 90°, 0.2 mm slit, step size of 0.02°, and counting time of 20 sec/step. According to the phase identification made by XRD the following parameters were considered for Rietveld refinement. The lattice constants of the hexagonal phase of $BaTi_{0.9}Rh_{0.1}O_{3\pm\delta}$ were calculated employing a modified model based on the crystallographic study of Ba(Ti, Pt)O_3 reported by Fischer and Tillmanns [14]. In the present study same space group P63/mmc was employed in the Rietveld model. The atoms positions occupied by Pt were replaced by Rh for the Rietveld model. The structural parameters for the $BaTiO_3$ tetragonal phase with the space group P4 mm reported by Kim et al. [15] were employed in the Rietveld model for the determination of the lattice constants. Finally, the structural model of Ba_2TiO_4 with space group Pnams determined by Bland [16] was employed in the calculations. After reduction, the cubic structure for Rh° with the space group Fm-3 m was included in the Rietveld model.

The SEM analysis was carried out with a Zeiss Ultra 55 microscope from Oxford Instruments.

Hydrogen temperature programmed (H_2-TPR) experiments were performed with a Quantachrome CHEMBET 3000 instrument. The powder sample (100 mg) was firmly placed in a U-tube within two plugs of quartz wool and was heated at a temperature range between 25 and 900 °C in 5 vol.% H_2/N_2 (25 ml × min^{-1}) at a rate of 5 °C × min^{-1}. The H_2 consumption was determined using a TCD detector. The X-ray absorption fine structure data were collected at the Rh K-edge ($E_0 = 23.22$ keV) at the SuperXAS beamline of the Swiss Light Source (Paul Scherrer Institute, Villigen, Switzerland) in transmission mode. Simulation of XANES spectra was performed using the FDMNES code [17]. The atomic cluster was generated using the ARTEMIS package [18] and replacing Ti atoms by Rh atoms in both crystallographic sites. Several simulations were performed in the crystallographic sites until convergence of the shape of the spectra ($R_{cluster} = 6.0$ Å). The final spectrum was obtained by summing the spectra obtained from both crystallographic sites with equal statistical weight.

3. Results and discussion

3.1. XRD and SEM-analysis

The XRD pattern of $BaTiO_3$ calcined at 1000 °C (Fig. 1) exhibits the tetragonal phase (JCPDS 005-0626) together with traces of a monoclinic phase $BaTi_2O_5$ (JCPDS 034-0133) and TiO_2 rutile (JCPDS 0211276). The reflection at $2\theta = 23.8°$ is related to $BaCO_3$ (JCPDS 045-1475) impurities. The phase composition and structure of pure $BaTiO_3$ remained unaffected after reduction at 700, 800 and 900 °C. Fig. 1 also shows that the difference between the XRD patterns of the fresh sample calcined at 1000 °C (oxidized state) and the sample after reduction at 900 °C (reduced state) is negligible. The white color of the initial $BaTiO_3$ oxide turned to gray implying a

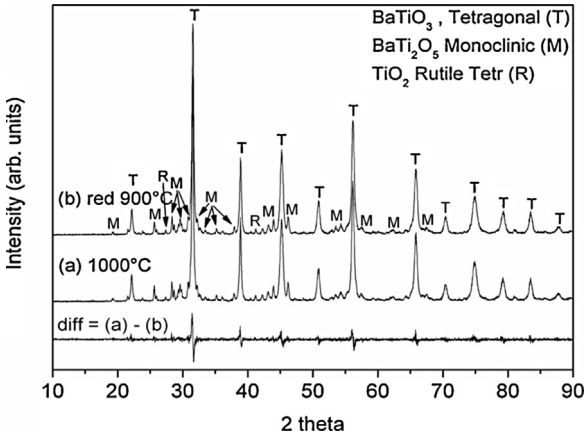

Fig. 1. XRD patterns of (a) fresh and (b) reduced $BaTiO_3$ in 2.5 vol.% H_2 + Ar. (c) is the difference pattern between (a) and (b).

slight reduction of the perovskite oxide. The reduction treatment produces an oxygen deficient $BaTiO_{3-x}$ perovskite and color change [19].

Fig. 2a displays the effect of the temperature and hydrogen containing atmosphere on the $BaTi_{0.9}Rh_{0.1}O_3$ perovskite. The XRD pattern of $BaTi_{0.9}Rh_{0.1}O_3$ calcined at 1000 °C is largely dominated by the reflections of the hexagonal phase (JCPDS 034-0129). Tetragonal $BaTiO_3$ (JCPDS 005-0626) is a minority phase. The absence of reflections of a Rh-containing phase and the stabilization of hexagonal $BaTiO_3$ compared to Rh-free $BaTiO_3$ indicate that rhodium likely replaces Ti atoms and is dissolved in the crystal lattice. Metal ions such as Ru, Rh, [20] and Fe, Pt [21] have been shown to stabilize the hexagonal phase of $BaTiO_3$. Similarly, Pd stabilizes hexagonal $YFeO_3$ and shifts the formation of the orthorhombic phase to higher temperature [22].

Clear phase transitions are observed upon reduction. A weak reflection appears at $2\theta = 47.74°$ after reduction at 700 °C, which is related to the formation of metallic fcc Rh° (JCPDS 005-0685). Simultaneously, two reflections at $2\theta = 28.6°$ and 29.2° reveal the formation of the orthorhombic *o*-Ba_2TiO_4 (JCPDS 038-1481) phase. Therefore, partial segregation of Rh is accompanied by a Rh-deficient $BaTiO_3$ phase (e.g. $BaTi_{0.9}Rh_{0.1-x}O_3$). Samples with lower Rh content ($BaTi_{0.95}Rh_{0.05}O_3$, $BaTi_{0.995}Rh_{0.005}O_3$; not shown) behave similarly after reduction. The observed phase transitions of $BaTi_{0.9}Rh_{0.1}O_3$ occur as a result of the segregation of Rh from the bulk of the perovskite oxide after the reduction treatment. Reduction at 800 °C and 900 °C caused further development of the orthorhombic phase at the expense of the hexagonal phase (see Fig. 2a).

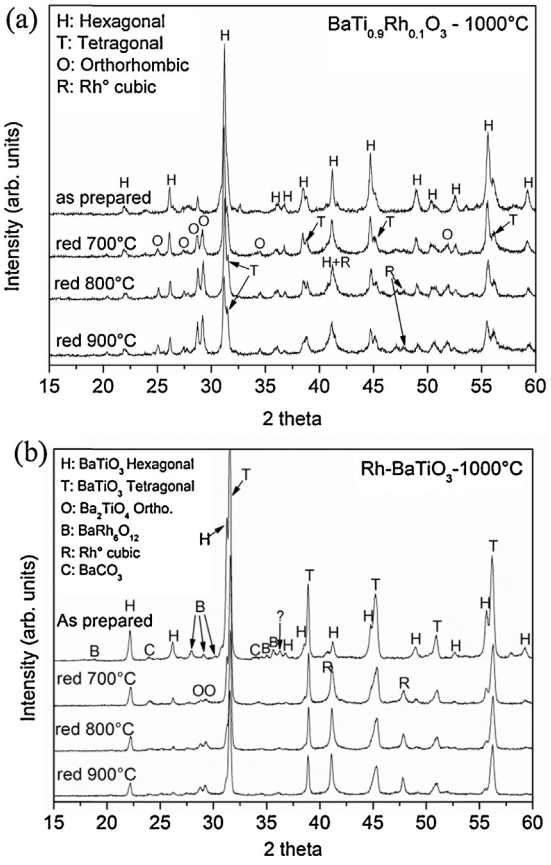

Fig. 2. XRD patterns of (a) $BaTi_{0.9}Rh_{0.1}O_3$ and (b) Rh–$BaTiO_3$-1000 °C after calcination at 1000 °C and after reduction at various temperatures in 2.5 vol.% H_2 + Ar.

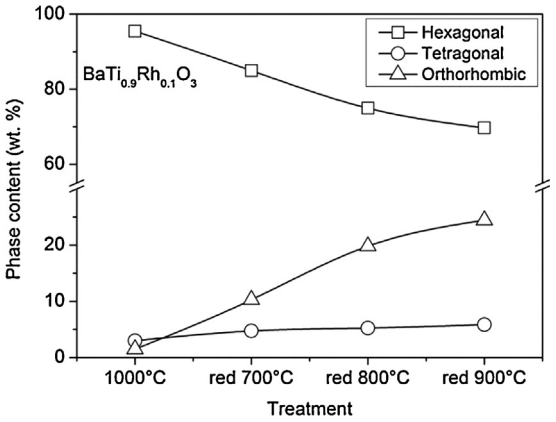

Fig. 3. Phase contents wt% of $BaTi_{0.9}Rh_{0.1}O_3$ after reduction in 2.5 vol.% H_2 + Ar at 700, 800 and 900 °C.

Rietveld refinement reveals that a considerable fraction of the hexagonal phase (ca. 54%) survives the reduction treatment at 900 °C (see Fig. 3). This is either a bulk phase containing Rh not accessible to hydrogen, or alternatively higher temperature, longer reduction time and higher hydrogen concentration are necessary to promote hydrogen diffusion and the complete reduction of the integrated Rh-ions. The lattice constants of the hexagonal perovskite obtained by Rietveld display only slight changes after reduction at 700, 800, and 900 °C (Table 1). The variation of the lattice constant *c* was only of 0.338% after reduction at 900 °C compared to the lattice constant of the perovskite calcined at 1000 °C. Similarly, only minor changes of the lattice parameters of the tetragonal structure were measured, a change becoming measurable only after reduction at 900 °C (0.207% for *a* and 0.347% for *c*), which might be related to the transition from the tetragonal into the cubic crystal phase. The lattice constants of these two structures are very close [15]. Finally, negligible changes of the lattice constants of the orthorhombic structure $BaTi_2O_4$ were detected in the same sample.

The tetragonal and the hexagonal $BaTiO_3$ phases are the main modifications of Rh–$BaTiO_3$ in the oxidized state observed by XRD (Fig. 2b). Note that the designation Rh–$BaTiO_3$ is only a representation of the system composition and indicates that this material was prepared by impregnation of $BaTiO_3$ followed by calcination. No Rh oxide phases could be detected in this sample suggesting that Rh is mainly dissolved in the $BaTiO_3$ lattice after impregnation with $Rh(NO_3)_3$ and calcination affording mainly the $BaTi_{0.9}Rh_{0.1}O_3$ hexagonal phase (JCPDS 034-0129). The presence of a small amount of $BaRh_6O_{12}$ (JCPDS 046-0962) indicates that some Rh segregated at the surface of $BaTiO_3$ and enriched the surface with Ba. Therefore, impregnation of $BaTiO_3$ with Rh produces two phases: the *h*-$BaTi_{0.9}Rh_{0.1}O_3$ and $BaRh_6O_{12}$.

The $BaRh_6O_{12}$ phase completely disappeared upon reduction while the *h*-$BaTi_{0.9}Rh_{0.1}O_3$ hexagonal phase gradually decreased upon reduction at 700, 800, and 900 °C, and the fraction of cubic Rh° and orthorhombic Ba_2TiO_4 phases increased with increasing

Table 1
Lattice constants of the hexagonal $BaTi_{0.9}Rh_{0.1}O_3$ perovskite calculated after Rietveld refinement; space group P63/mmc, step size = 0.02°, and counting time = 20 sec/step.

Treatment	*a*(Å)	*c*(Å)
Calcined,1000 °C[a]	5.7195	14.0179
Reduced, 700 °C	5.7214	14.0135
Reduced, 800 °C	5.7228	14.0169
Reduced, 900 °C	5.7295	13.9705

[a] Initial, after calcination.

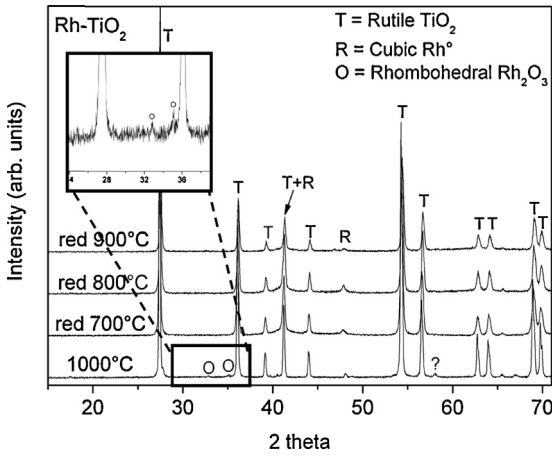

Fig. 4. XRD patterns of fresh and reduced Rh–TiO_2.

reduction temperature (Fig 2b). The intense XRD-reflections of Rh° indicate the presence of high metal concentration on the perovskite oxide surface.

After calcination at 1000 °C, the XRD of Rh–TiO_2 displayed predominantly the rutile phase (JCPDS 021-1276; Fig. 4). Weak reflections of rhombohedral Rh_2O_3 (JCPDS 041-0541) are also observed. Upon reduction at 900 °C, the reflections of the Rh_2O_3 vanished and the metallic Rh° formed.

The changes of the nano-structure of $BaTi_{0.9}Rh_{0.1}O_3$ captured by XRD after reduction at 900 °C were also imaged by using FE-SEM. Fresh $BaTi_{0.9}Rh_{0.1}O_3$ is characterized by small (80–240 nm) and larger (ca. 400 nm) grains (Fig. 5a1). Only after reduction at 900 °C, a phase consisting of very small particles (5–16 nm) becomes visible on the large grains of $BaTi_{0.9}Rh_{0.1}O_3$ (Fig. 5b1). This FE-SEM image visually corroborates the formation of Rh° nano-particles observed by XRD. The morphology differences of $BaTi_{0.9}Rh_{0.1}O_3$ (predominantly hexagonal) and Rh–$BaTiO_3$ (tetragonal) are clearly observed by FE-SEM (Fig. 5a1 and a2).

3.2. Temperature programmed reduction

The reducibility of the samples was also investigated by using H_2-TPR in order to support the XRD characterization (Fig. 6). Reduction of $BaTiO_3$ occurs at temperatures higher than 600 °C. In agreement with the XRD data, the signal is assigned to the formation of orthorhombic $BaTi_2O_4$ phase. Reduction of supported Rh_2O_3 is represented by the TPR profile of Rh–TiO_2 exhibiting a strong reduction signal between 200 °C and 300 °C. The addition of Rh to $BaTiO_3$ increases the reducibility of $BaTiO_3$ and causes the appearance of reduction events at low temperatures. A peak is observed at 236 °C that is followed by a broad hydrogen consumption extending up to 850 °C. The TPR profile of Rh–$BaTiO_3$ exhibits two clear and sharp reduction peaks at 168 °C and 227 °C that are assigned to reduction of the oxidized Rh phase (not observed in the XRD) and Rh in strong interaction with $BaTiO_3$ and

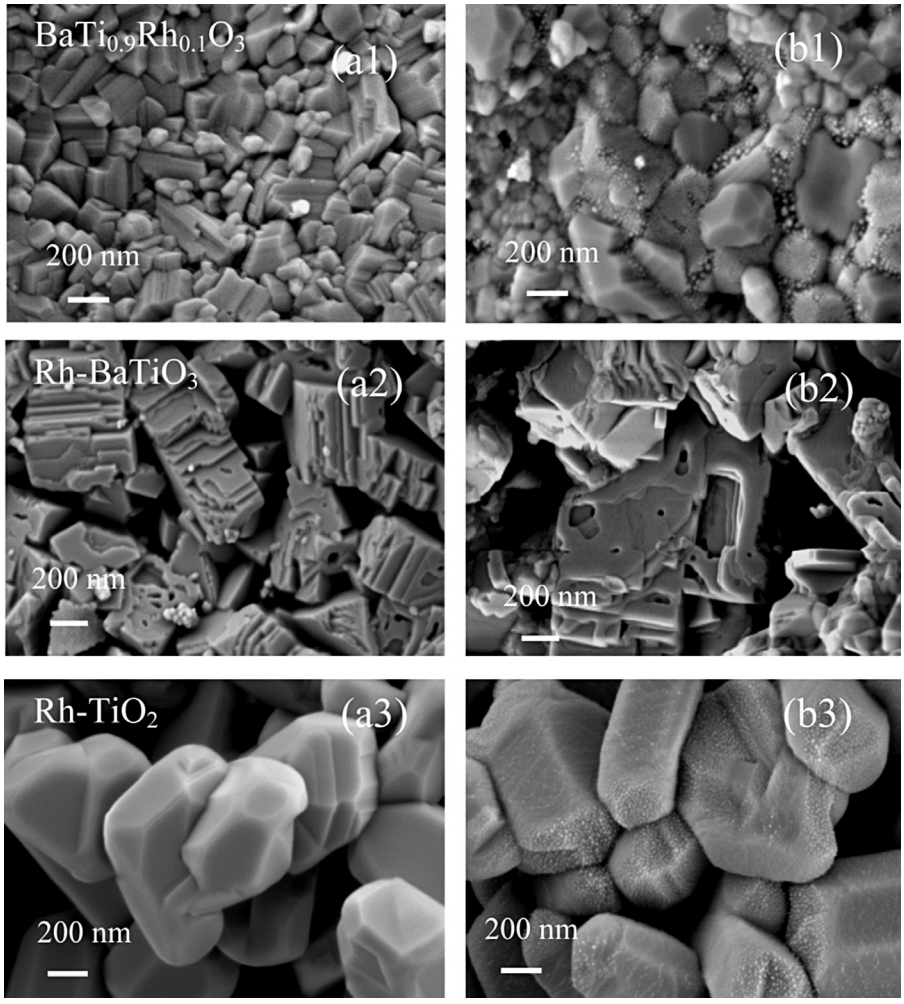

Fig. 5. FE-SEM micrographs of $BaTi_{0.9}Rh_{0.1}O_3$, Rh–$BaTiO_3$ and Rh–TiO_2 (a) after calcination at 1000 °C and after reduction in 2.5 vol.% H_2 + Ar at 900 °C (b).

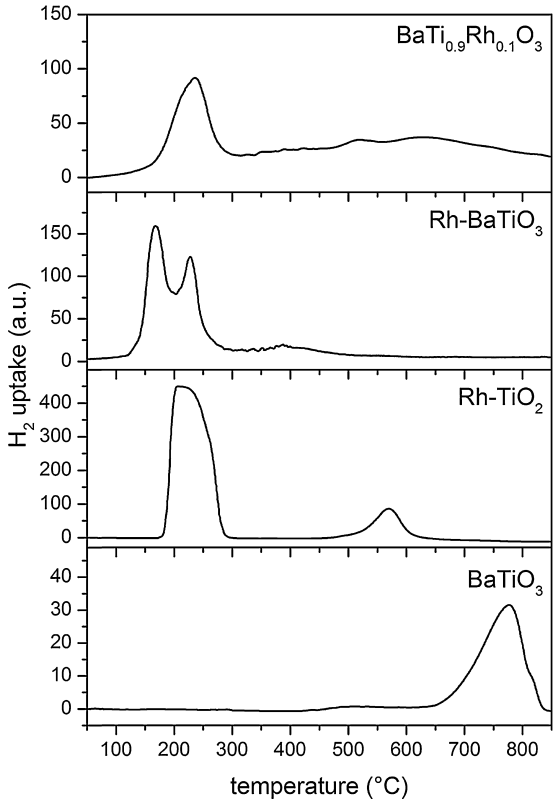

Fig. 6. H_2-TPR profiles of Rh containing oxides.

$BaTi_{0.9}Rh_{0.1}O_3$, respectively. Therefore, comparison between the reduction characteristics of $BaTi_{0.9}Rh_{0.1}O_3$ and Rh–$BaTiO_3$ reveals that the signal at 236 °C of $BaTi_{0.9}Rh_{0.1}O_3$ can be attributed to reduction of lattice Rh. The reduction events at higher temperature may be related to the further phase transition observed in Fig. 1 of the hexagonal phase to the tetragonal phase.

3.3. The coordination state of Rh in $BaTi_{0.9}Rh_{0.1}O_3$

The coordination state and atomic environment of Rh was studied using X-ray absorption spectroscopy. Fig. 7 shows the normalized XANES spectra of $BaTi_{0.9}Rh_{0.1}O_3$ and Rh–TiO_2 at the Rh K-edge (E_0 = 23.22 keV). For the sake of clarity Rh_2O_3 and the Rh foil were also measured. The XANES spectrum of $BaTi_{0.9}Rh_{0.1}O_3$ presents a clear peak at 10.4 eV above the white line (arrow) that is not present in the XANES spectrum of Rh_2O_3 or supported Rh in Rh–TiO_2. This feature indicates a peculiar coordination of Rh. Additional spectral differences are visible at higher energy. Therefore, the XANES spectra of $BaTi_{0.9}Rh_{0.1}O_3$ were simulated by considering that Rh could occupy two different octahedral Ti^{4+} sites of $BaTiO_3$. The hexagonal structure of $BaTiO_3$ (P6/3mmc) was used for the simulation, since the XRD data clearly showed the preferential growth of this phase when Rh is directly added to the precursors solution (Fig. 1). The simulated spectra at the Rh K-edge (Fig. 7) also exhibit a doublet around the white line but with different intensity with respect to the experimental spectrum. The presence of the feature at the same energy and with higher intensity than the white line provides evidence that Rh occupies the Ti site in $BaTi_{0.9}Rh_{0.1}O_3$ and is therefore finely (atomically) distributed within the $BaTiO_3$ lattice.

The k^3-weighted Fourier transform of the EXAFS spectra of the various samples is shown in Fig. 8. Clearly, beside the main first-shell coordination of Rh (Rh–O), Rh–TiO_2 presents features corresponding to those of the hexagonal Rh_2O_3 phase thus

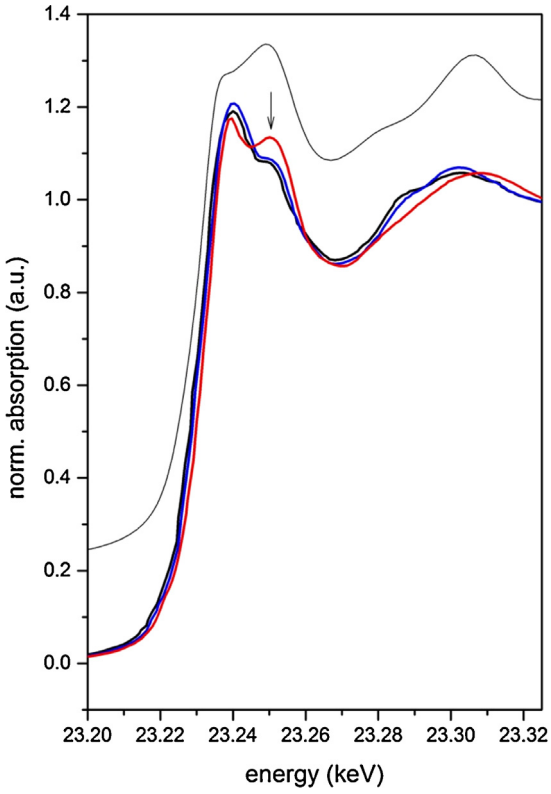

Fig. 7. Normalized Rh K-edge XANES spectra of $BaTi_{0.9}Rh_{0.1}O_3$ (red), Rh–TiO_2 (blue) and Rh_2O_3 (black) together with the simulated spectrum of $BaTi_{0.9}Rh_{0.1}O_3$ assuming Rh occupancy of the Ti^{4+} octahedral sites. The arrow indicates the additional peak discussed in the text. (For interpretation of the references to color in this figure legend, the reader is referred to the web version of this article.)

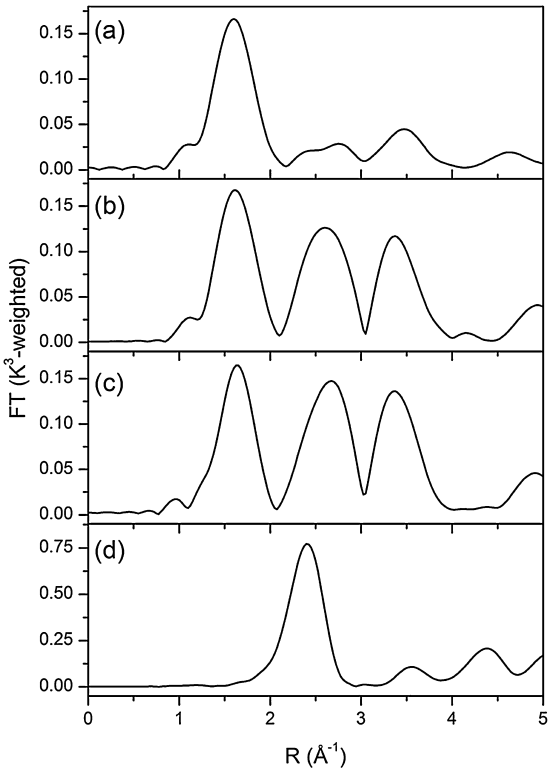

Fig. 8. Non-phase shift corrected Fourier transformed EXAFS data of (a) $BaTi_{0.9}Rh_{0.1}O_3$, (b) Rh-TiO_2, (c) Rh_2O_3 and (d) Rh foil.

confirming that impregnation with the Rh precursor provides bulk Rh_2O_3-like particles. This phase accounts for the reduction peak at ca. 200 °C (Fig. 6). On the contrary, no defined second shell can be observed in the case of $BaTi_{0.9}Rh_{0.1}O_3$ thus supporting the very fine dispersion of Rh within the sample after calcination at 1000 °C. The weak signals at ca. 3 and 3.5 $Å^{-1}$ could be tentatively attributed to the coordination to Ti or Ba.

The possibility that Rh coordinates in the octahedral Ti^{4+} sites is demonstrated by the XANES spectra of the $CaTi_{0.95}Rh_{0.05}O_3$ measured by Naito et al. [2,12] and by the analog Pd-containing samples, e.g. $LaFe_{0.95}Pd_{0.05}O_3$ and $LaCo_{0.95}Pd_{0.05}O_3$ [9,10]. Hence, the octahedral coordination of Pd and Rh in the perovskite-type lattice produces a characteristic white line shape.

3.4. Conclusions

$BaTi_{0.9}Rh_{0.1}O_{3\pm\delta}$ perovskite-type oxides with Rh in the perovskite lattice were prepared by a soft chemistry method using organic Ba-acetate and Ti-isopropoxide salts as precursors. These salts are easily dissolved in acetic acid and isopropanol, respectively. The inorganic source of Rh, $Rh(NO_3)_3$ did not disturb the synthesis of the Rh-containing perovskite-like oxide. The addition of the acetyl acetonate solvent clearly improved the solution formation, which is a key step for the synthesis of precious metals in solid solution with perovskite-type oxides.

The synthesis method allowed Rh to disperse homogeneously in the perovskite lattice, whereas no other Rh-oxide could be found by XRD analysis. The EXAFS study of $BaTi_{0.9}Rh_{0.1}O_3$ confirms both the fine dispersion of Rh and the coordination in the $BaTiO_3$ lattice, thus the formation of a solid solution. The presence of Rh in the perovskite stabilizes the hexagonal modification and the reduction treatment causes its decomposition into the orthorhombic phase $BaTi_2O_4$ and Rh°, thus suggesting a new mechanism for Rh segregation from the perovskite.

A different situation is obtained in the case of perovskite supported Rh (Rh–$BaTiO_3$). During calcination at 1000 °C of Rh $(NO_3)_3$ impregnated on $BaTiO_3$, prepared at 1000 °C, a similar reaction as in the $BaTi_{0.9}Rh_{0.1}O_3$ occurs. Rhodium diffuses into the tetragonal $BaTiO_3$ and induces the tetragonal to the hexagonal phase transition. Traces of $BaRh_6O_{12}$ observed in XRD indicate that the large excess of Rh (10 wt%) provokes the formation of a Rh-containing phase on the outer surface of the perovskite oxide. $BaRh_6O_{12}$ completely disappears after reduction, which is accompanied by a decrease of the hexagonal phase and the appearance of cubic Rh°. The high amount of the $BaTiO_3$ tetragonal phase indicates that the surface reaction between Rh and $BaTiO_3$ was possible only to some extent. Bulk tetragonal $BaTiO_3$ prepared at 1000 °C is likely less inaccessible to the Rh-solution, whereas direct addition of the Rh precursor to the $BaTiO_3$ precursor salts and generation of a clear solution integrates Rh homogeneously within $BaTiO_3$ and stabilizes the hexagonal phase.

References

[1] R.L.H. Voorhoeve, Perovskite-related oxides as oxidation-reduction catalysts, in: J.J. Burton, R.L. Garten (Eds.), Advanced Materials in Catalysis, Academic Press: Linden, New Jersey, 1977.
[2] H. Tanaka, M. Uenishi, M. Taniguchi, I. Tan, K. Narita, M. Kimura, K. Kaneko, Y. Nishihata, J. Mizuki, Catal. Today 117 (2006) 321–328.
[3] Y. Nishihata, J. Mizuki, H. Tanaka, M. Uenishi, M. Kimura, J. Phys. Chem. Solids 66 (2005) 274–282.
[4] M. Uenishi, M. Taniguchi, H. Tanaka, M. Kimura, Y. Nishihata, J. Mizuki, T. Kobayashi, Appl. Catal. B 57 (2005) 267–273.
[5] M. Uenishi, H. Tanaka, M. Taniguchi, I. Tan, Y. Nishihata, J. Mizuki, T. Kobayashi, Catal. Commun. 9 (2008) 311–314.
[6] H. Tanaka, M. Misono, Current opinion solid state, Mater. Sci. 5 (2001) 381–387.
[7] G.C. Mondragón Rodríguez, R. Ochrombel, B. Saruhan, J. Eur. Ceram. Soc. 28 (2008) 2611–2616.
[8] G.C. Mondragón Rodríguez, K. Kelm, B. Saruhan, Appl. Catal. A 387 (2010) 173–184.
[9] A. Eyssler, P. Mandaliev, A. Winkler, P. Hug, O. Safonova, R. Figi, A. Weidenkaff, D. Ferri, J. Phys. Chem. C 114 (2010) 4584–4594.
[10] A. Eyssler, A. Winkler, O. Safonova, M. Nachtegaal, S.K. Matam, P. Hug, A. Weidenkaff, D. Ferri, Chem. Mater. 24 (2012) 1864–1875.
[11] H. Tanaka, M. Taniguchi, M. Uenishi, N. Kajita, I. Tan, Y. Nishihata, J. Mizuki, K. Narita, M. Kimura, K. Kaneko, Angew. Chem. 118 (2006) 6144–6148.
[12] K. Naito, H. Tanaka, M. Taniguchi, M. Uenishi, I. Tan, N. Kajita, I. Takahashi, SAE Techinical Paper 2006-01-0851, (2006) , pp. 19–26.
[13] G.C. Mondragón Rodríguez, Y. Gönüllü, B. Saruhan, Top. Catal. 56 (2013) 397–404.
[14] R. Fischer, E. Tillmanns, Z. Kristallogr. 157 (1981) 69–81.
[15] Y.I. Kim, J.K. Jung, K.S. Ryu, Mater. Res. Bull. 39 (2004) 1045–1053.
[16] J.A. Bland, Acta Crystallogr. 14 (1961) 875–881.
[17] Y. Joly, Phys. Rev. 63 (2001) p. 125120-10.
[18] B. Ravel, M. Newville, Athena, Artemis, Hephaestus, data analysis for X-ray absorption spectroscopy using IFEFFIT, J. Synchrotron Radiat. 12 (2005) 537–541.
[19] H. Arend, P. Coufová, J. NováK, Chemical J. Am. Ceram. Soc. 50 (1967) 22–25.
[20] J.G. Dickson, L. Katz, R. Ward, J. Am. Chem. Soc. 83 (1961) 3026–3029.
[21] H. Arend, L. Kihlborg, J. Am. Ceram. Soc. 52 (1969) 63–65.
[22] J. Li, U.G. Singh, J.K. Schladt, J.K. Stalick, S.L. Scott, R. Seshadri, Chem. Mater. 20 (2008) 6567–6576.